Bioactive Materials 6 (2021) 3608–3619

Contents lists available at ScienceDirect

Bioactive Materials

journal homepage: www.sciencedirect.com/journal/bioactive-materials

Regulation of cell locomotion by nanosecond-laser-induced hydroxyapatite patterning

Seung-Hoon Um [a,b], Jaehong Lee [a], In-Seok Song [c], Myoung-Ryul Ok [a], Yu-Chan Kim [a,d], Hyung-Seop Han [a,*], Sang-Hoon Rhee [b,**], Hojeong Jeon [a,d,e,***]

[a] Center for Biomaterials, Biomedical Research Institute, Korea Institute of Science and Technology (KIST), Seoul, 02792, Republic of Korea
[b] Department of Dental Biomaterials Science, Dental Research Institute, School of Dentistry, Seoul National University, Seoul, 03080, Republic of Korea
[c] Department of Oral and Maxillofacial Surgery, Korea University Anam Hospital, Seoul, 02841, Republic of Korea
[d] Division of Bio-Medical Science and Technology, KIST School, Korea University of Science and Technology, Seoul, 02792, Republic of Korea
[e] KU-KIST Graduate School of Converging Science and Technology, Korea University, Seoul, 02841, Republic of Korea

ARTICLE INFO

Keywords:
Nanosecond laser
Laser engraving
Hydroxyapatite patterning
Cell migration control
Cell tracking

ABSTRACT

Hydroxyapatite, an essential mineral in human bones composed mainly of calcium and phosphorus, is widely used to coat bone graft and implant surfaces for enhanced biocompatibility and bone formation. For a strong implant–bone bond, the bone-forming cells must not only adhere to the implant surface but also move to the surface requiring bone formation. However, strong adhesion tends to inhibit cell migration on the surface of hydroxyapatite. Herein, a cell migration highway pattern that can promote cell migration was prepared using a nanosecond laser on hydroxyapatite coating. The developed surface promoted bone-forming cell movement compared with the unpatterned hydroxyapatite surface, and the cell adhesion and movement speed could be controlled by adjusting the pattern width. Live-cell microscopy, cell tracking, and serum protein analysis revealed the fundamental principle of this phenomenon. These findings are applicable to hydroxyapatite-coated biomaterials and can be implemented easily by laser patterning without complicated processes. The cell migration highway can promote and control cell movement while maintaining the existing advantages of hydroxyapatite coatings. Furthermore, it can be applied to the surface treatment of not only implant materials directly bonded to bone but also various implanted biomaterials implanted that require cell movement control.

1. Introduction

Hydroxyapatite (HA), composed of calcium and phosphoric acid as mineral components of human bone, is often applied to the surface of materials in a clinical setting that require direct bonding to bone [1,2]. A good record of favorable clinical outcomes has made HA one of the most common implant coating materials for increasing the bonding strength of dental and orthopedic implants [3–6]. Artificial materials implanted into the body to bond to bone undergo a sequence of attachment involving serum proteins, immune cells, and stem cells, followed by osteoblast differentiation and bone cell growth for new bone formation [7,8]. In recent years, research has been conducted on promoting bone formation by implementing a surface that can promote bone-forming cell adhesion [9–11]. This is partly because the bone-bonding and forming capability of titanium (Ti) and its alloys, some of the most common materials for implant devices, is insufficient compared with that of autologous bones. Therefore, the utilization of HA coatings to promote osteoblast adhesion and bone formation has been explored [12,13] and applied in clinical practice [14–17].

Research on surface modifications that can control cell migration is also underway since it is well known that new bone formation requires both cell attachment [18–21] and cell movement to reach the bone formation site [22–24]. In particular, it has been reported that bone formation-related genes such as Runx2, osteocalcin, and osteopontin are

Peer review under responsibility of KeAi Communications Co., Ltd.
* Corresponding author.
** Corresponding author.
*** Corresponding author. Center for Biomaterials, Biomedical Research Institute, Korea Institute of Science and Technology (KIST), Seoul, 02792, Republic of Korea.
E-mail addresses: hynhan@kist.re.kr (H.-S. Han), rhee1213@snu.ac.kr (S.-H. Rhee), jeonhj@kist.re.kr (H. Jeon).

https://doi.org/10.1016/j.bioactmat.2021.03.025
Received 24 January 2021; Received in revised form 9 March 2021; Accepted 9 March 2021

expressed and calcium deposition of osteoblasts is increased on the surface where cell migration is promoted [25,26] to result in increased osseointegration [18]. Several studies have explored controlling the movement of cells using surface patterns [27–29]. However, most studies have used relatively easy-to-process polymer materials [30,31]. Even when HA is used, a complex additional process is required, such as reproducing the pattern by placing HA powder in the patterned frame followed by heat treatment [32,33]. Furthermore, most previous studies have focused on cell shape and proliferation [34,35], while there is a lack of research on surface patterns that can control the movement of bone-forming cells on the HA surface, where bone cells directly bond and form new bone.

In this study, a method to create a cell migration highway (CMH) pattern was developed using simple nanosecond laser processing to control cell movement on the surface of HA. This method, which does not require complicated additional steps, applies nanosecond laser engraving [36] directly to the HA surface to expose the base material while creating road-like patterns. By allowing different materials to be exposed together, this technique affords a topographical effect and simultaneously provides the benefits from the exposure of two different material surfaces. We applied and developed the results of our existing research that can coat HA using a nanosecond laser [37] to form various types of HA patterns. This new technique promotes and controls cell migration while maintaining the advantages of the existing apatite, and it is applicable to all areas where such apatite is used. The implementation and microstructure of the CMH were confirmed through electron microscopy and 3D topographical analysis. In-depth cellular evaluation of the CMH visualized the controlled cell migration and adhesion using osteogenic cells. The principle underlying the controlled cellular behavior by the application of the CMH was explored through serum protein adhesion, live-cell imaging, cell tracking, and quantification analysis.

2. Materials and methods

2.1. Preparation of CMH

To implement the CMH, titanium (grade 5, Ti–6Al–4V, 2.5 mm thick, 10 mm wide, 10 mm long) specimens were polished with #600 grit using a surface polishing machine (M-PREP 5, ALLIED, USA) and ultrasonically cleaned in the order of distilled water, 70% EtOH (64-17-5, DUKSAN, Korea), 99.8% EtOH (64-17-5, DUKSAN, Korea), and distilled water (Pure Power I, Human Corp. Korea) for 10 min each. The washed specimen was stored in a desiccator at room temperature until the experiment.

A nanosecond laser (ytterbium fiber laser, 1065 nm, Laservall, China) was used to coat HA on the specimen surface. A precursor solution was prepared using Dulbecco's modified Eagle's medium (LM001-05, WELGENE, Korea), $Ca(NO_3)_2$ (C4955, Sigma-Aldrich, USA), and H_3PO_4 (P5811, Sigma-Aldrich, USA). The specimen was immersed in the precursor solution, and a nanosecond laser was used to irradiate the surface. The detailed composition and laser irradiation conditions of the reaction solution for the HA coating were selected by referring to the LISSC method [34]. Briefly, for the HA coating, the laser settings were a power of 10 W, pulse duration of 200 ns, repetition rate of 500 kHz, and scanning speed of 0.5 m/s. In all laser processes, before irradiating the specimen, the laser output was measured with a power meter (Nova II, Ophir, Israel), and then the experiment was conducted. For the HA1 and HA2 specimens, the apatite coating thickness was controlled to 16.8 ± 7.3 and 47.5 ± 12.7 μm by setting the number of loops (number of repeated laser irradiations) to 50 and 100, respectively.

For CMH formation, the HA-coated specimen was immersed in distilled water and irradiated with the nanosecond laser under the conditions of 10 W power, 100 mm/s speed, 1000 kHz frequency, 200 ns pulse width, 10 μm line gap, and 10 loops. The specimens on which a CMH was formed were ultrasonically cleaned for 10 min each in the order of distilled water, 70% EtOH, 99.8% EtOH, and distilled water, then stored in a desiccator before experiments.

2.2. Characterization of CMH microstructure and topography

The microstructure of the laser-treated titanium and CMH-embedded HA specimens were analyzed using electron and optical microscopy. Microstructural analysis was performed using a scanning electron microscope (SEM; Inspect F50, FEI, USA) after the sample surface was coated with platinum for 60 s at 15 mA using an ion coater (MC1000, Hitachi, Japan). For optical microscopic analysis, titanium, HA-coated specimens, and laser-processed specimens were prepared. Two-dimensional natural-color images were obtained to confirm each specimen size and color, and 3D images were measured together to determine the surface topography. Both the optical and 3D topography measurements were performed using a 3D microscope (LSM-5000, Olympus, Japan). Surface roughness was determined using a surface analysis program (AnalysisApp, Olympus, Japan) after obtaining topography data from each specimen with the 3D microscope. For statistical significance analysis, measurements of 10 or more specimens were performed for each condition, and the raw data, mean, and standard deviation are given. In addition, to determine the change in surface roughness due to laser processing, the laser-processed part of each specimen was marked, and the surface roughness according to analysis location was also determined.

2.3. Osteoblast adhesion and migration analysis

For cell experiments, mouse-derived osteoblasts (MC3TC-E1, ATCC, USA) were used. All cells used in the experiments were stored in −196 °C liquid nitrogen, thawed in a 37 °C constant-temperature water bath one day before the experiment, and then dispensed into a tissue culture plate with a 10 cm diameter (100 mm × 20 mm, Corning, USA) and incubated (Thermo Fisher Scientific Forma, USA) for one day for cell stabilization. To evaluate cell adhesion and migration, a mixture of minimum essential medium (Alpha-MEM, Hyclone, USA), 10 v/v% fetal bovine serum (SH30088.03, Hyclone, USA), and 1% antibiotic (penicillin-streptomycin, Thermo Fisher Scientific, USA) was used as a cell culture solution. The specimen was placed in a 24 well plate (Corning, USA) with a size of 1 cm × 1 cm, and 5×10^5 cells were dispersed in 1 ml of cell culture solution and then poured into the specimen to submerge it. After incubation at 37 °C, 5% CO_2, and 95% humidity for 24 h, the cells were washed three times with phosphate-buffered saline (PBS, pH 7.4, Gibco, USA) and fixed with a solution of 4% paraformaldehyde in PBS. Subsequently, the cytoplasms and nuclei were fluorescence-stained using rhodamine-phalloidin (R415, Invitrogen, USA) and DAPI (LS-J1033, Vectashield, USA), and images were taken with a fluorescence microscope (Axio Scope Imager A2M, ZEISS, Germany).

From the images of the cell nuclei (blue color), the number of cells and location information on the *x*- and *y*-axes were obtained using the ImageJ program (NIH, USA). The moving distance of the cells was masked before cell attachment. The locations where cell attachment did not occur were considered the cell migration starting point. After removing the masking, the cells were cultured for 24 h, and the location in the masked area was considered the final migration location. The data quantified using the *x*-and *y*-axis positional information were arranged with the Microsoft Excel program, and the graphs and statistical significance were analyzed using the Origin program (Origin 2.0, OriginLab, USA) (Fig. S2).

The relative cell density of cell adhesion and migration was determined using the location information on the *x*- and *y*-axes obtained by the above method. The number of adhered cells per unit area was measured, and the relative density according to location was calculated as a percentage and expressed as a diagram. The relative density was mapped by dividing the laser-processed portion and the unprocessed area. In addition, to check whether the relative cell density differed

significantly with the target location, a statistical significance test was conducted to distinguish the difference to the location when the laser-processed or unprocessed area are displayed together on a graph.

2.4. Real-time observation and tracking of live cells

To analyze the cell behavior in real time, a cover glass (thickness 0.13 mm, diameter 25 mm, borosilicate glass DIN ISO 8255, Marienfeld, German) capable of transmitting light during microscopy was used. An HA coating and CMH were implemented on the glass surface using the LISSC method and laser engraving mentioned in Section 2.1. HA debris on the sample surface was washed using 70% EtOH (64-17-5, DUKSAN, Korea), 99.8% EtOH (DUKSAN, Korea), and distilled water (Pure Power I, Human Corp., Korea) and stored in a dryer until the experiment. The prepared sample was placed in a 6 well plate (Corning, USA), and 5×10^4 cells/well were seeded. After placing in a chamber at 37 °C, 5% CO_2, and 95% or greater humidity, the cells were allowed to stand for 10 min to stabilize. A total of 288 images were obtained at 5 min intervals for 24 h using a phase difference method with a live cell microscope (Axio Observer Z1, Zeiss, Germany). In all the acquired images, each cell location was identified and tracked using a cell tracking program (CellTracker) [38]. After obtaining the information to be considered X (x-axis position), Y (y-axis position), and Z (measured time) of all cells in each image (5 min per frame), the data were organized with Excel, and Origin was used to create a chart and to test for statistical significance. The HA region, CMH region, and interface between the two were presented together using the 288 images at 30 fps to observe the cell movement over 24 h.

2.5. Analysis of serum protein adhesion according to CMH implementation

To analyze the serum protein adhesion characteristics, specimens of HA1, HA2, and HA2 with a CMH were prepared. The CMH was implemented using the LISSC and laser engraving method described in Section 2.1. A solution for protein adhesion was prepared by mixing mouse serum (#10410, Invitrogen, USA) with a cell culture medium (Alpha-MEM, Hyclone, USA) to a 10 v/v% concentration. A specimen was placed on a 6 well plate (Corning, USA), and 3 ml/well of the above solution was added to completely precipitate the specimen. Subsequently, the sample was maintained for 1 h in an environment of 37 °C, 5% CO_2, and 95% or greater humidity for the proteins to adhere to the specimen surface. The 6 well plate solution was removed, and PBS was added at 4 ml/well, maintained for 5 min, and removed. This process was repeated a total of 3 times to remove excess proteins not attached to the surface. Staining was performed using fibronectin antibody (ab2413, Abcam, England) and vitronectin antibody (ab45139, Abcam, England), and images were obtained using fluorescence microscopy. The fluorescence intensities of the HA and CMH regions in the fluorescence images were analyzed using ImageJ and are presented as relative values for each area. To analyze the total amount of attached serum proteins, CMH, HA1, and HA2 specimens with a size of 10 mm × 10 mm were prepared. Serum protein adhesion was carried out in the same manner as mentioned above, after which RIPA buffer (#89900, Thermo, USA) was added at 4 °C for 10 min to obtain the proteins attached to the surface. The protein amounts obtained from each sample surface were calculated by measuring the absorbance at a wavelength of 562 nm (GloMax GM3000, Promega, USA) using the micro-BCA (#23235, Thermo, USA) method.

2.6. Statistical significance analysis

Raw data are presented in all graphs showing the statistical analysis results. The statistical analysis method used for each graph is described in each figure caption. The Origin program was used for all statistical analyses. The statistical significance between groups was tested by ANOVA, and the significance analysis between each item was expressed using the Tukey post-test results. Data represent raw data, while *, **, and *** indicate statistically significant differences between each comparison group, with $^*P < 0.05$, $^{**}P < 0.01$, and $^{***}P < 0.001$.

3. Results

3.1. Implementation of CMH

A nanosecond laser was used to create a passageway to promote cell migration on the surface of an HA coating on titanium (Fig. 1a). The passageway was patterned so that the base Ti material was completely exposed through laser engraving on the surface coated with HA. In addition, a Ti surface without the HA coating was engraved under the same laser conditions to distinguish the difference in cell migration characteristics resulting from the combination of topography and materials. The effect of the width of the moving passage on the cell behavior was also determined by adjusting the width during the laser engraving process (Fig. 1b, d).

As shown in Fig. 1c and e, observation of the surface of each specimen subjected to laser engraving with SEM, optical microscopy, and 3D microscopy confirmed the formation of passageways with a controllable width. In subsequent descriptions, the passageway implemented on the Ti surface without an HA coating is termed “laser engraving,” while the road shape implemented on the HA surface is termed the CMH.

3.2. Inhibition of bone cell migration by HA

Cell migration analysis was performed to determine the inhibition of bone cell movement on the HA surface. Ti and HA specimens with different coating thicknesses (HA1: HA thickness, 16.8 ± 7.3 μm; HA2: HA thickness, 47.5 ± 12.7 μm) were prepared to determine the effect of HA thickness. Osteoblasts were dispensed on the surface of each sample and cultured for 24 h to compare the migration patterns (Fig. 2a). Fluorescently stained cytoplasms (orange color) compared in terms of both 2D images and 3D fluorescence intensity showed that the osteoblasts on the Ti surface migrated to cover the widest area, whereas the osteoblasts on HA1 and HA2 were only able to move and cover a much narrower area (Fig. 2b). The cytoplasmic fluorescence intensity distribution analysis based on the cell migration distance from the starting position showed that the fluorescence intensity of the cells on the Ti surface gradually started to decrease at approximately 2500 μm (Fig. 2c). In contrast, the fluorescence on HA1 and HA2 began to decrease significantly at approximately 1300 μm (Fig. 2d and e). A similar trend of cell migration inhibition on the HA1 and HA2 surfaces was also observed in the statistical significance analysis of the cell migration distance compared with the Ti surface (Fig. 2f).

3.3. Changes in cell adhesion characteristics by implementation of CMH

The effect of the CMH on cell adhesion was confirmed by comparing the number and location of adhered cells according to the presence or absence of a CMH. Cells were coated on the laser-engraved Ti surface specimen and on the CMH on the HA surface, followed by incubation for 24 h, after which the cell adhesion patterns were compared (Fig. 3a). Fluorescent staining of the cell nuclei (DAPI, blue) and cytoplasms (Actin, red) to observe the cells attached on the specimen surface showed no significant difference in osteoblast adhesion on the Ti surfaces with and without the laser engraving area or with different engraving widths (Fig. 3b). In contrast, on the surface with the CMH, more cells were attached to the HA area than to the CMH area (Fig. 3c).

The cells attached to the laser-engraved area on Ti (yellow dots) and to the non-engraved area (gray dots) are shown as a distribution chart in Fig. 3d. In terms of the number of cells attached per unit area, there was no difference between the two areas, as shown in Fig. 3e. In contrast, the distribution and density of cells attached to the CMH region of the HA

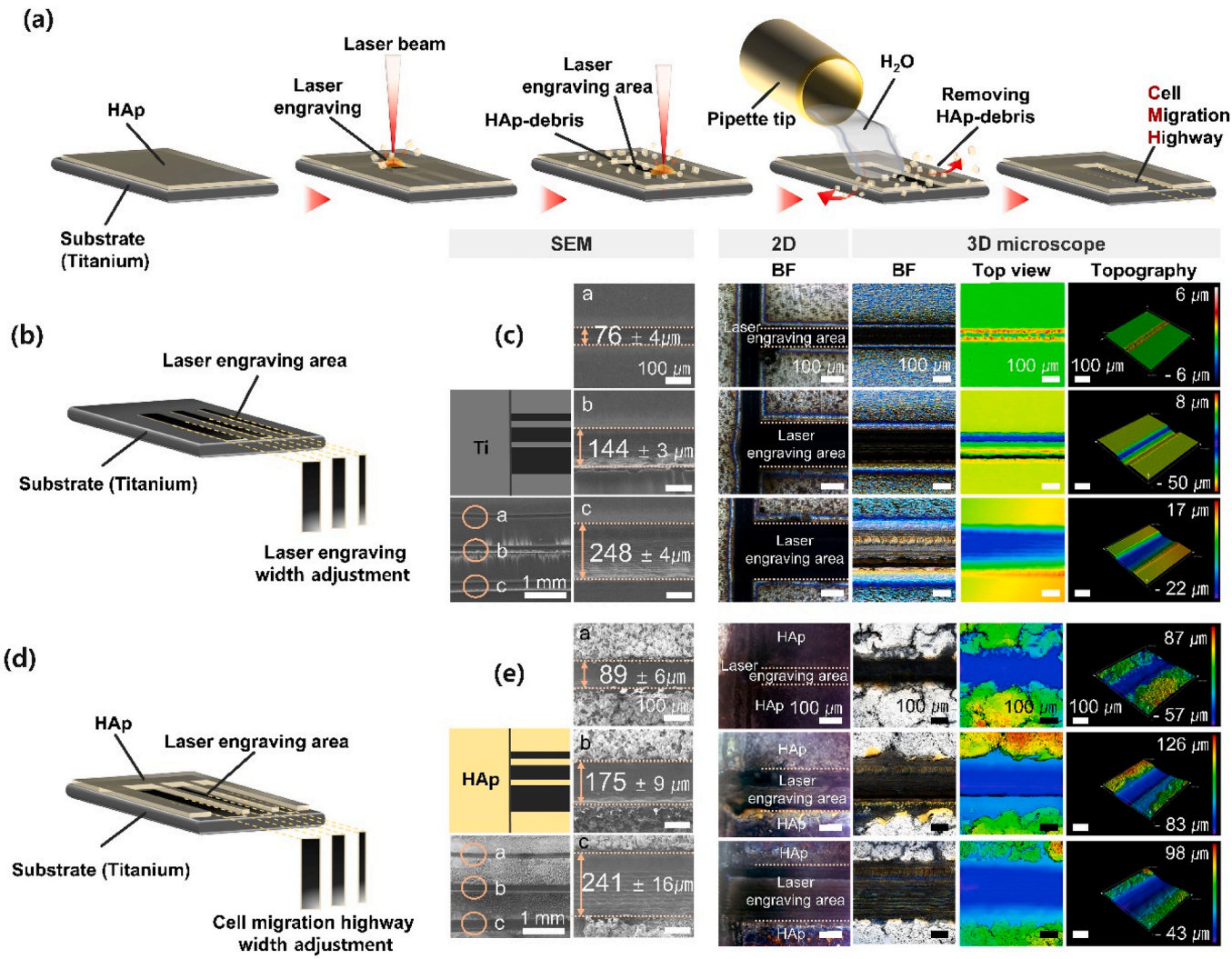

Fig. 1. Cell migration highway (CMH) implementation and microstructure analysis using nanosecond laser. (a) Schematic diagram of CMH implementation on the surface of hydroxyapatite using nanosecond laser. (b) Schematic diagram of laser engraving treatment on titanium surface. (c) Surface microstructure of laser engraved titanium surface using SEM, optical and 3D microscopes. (d) Schematic diagram of cell migration highway formation on the hydroxyapatite through laser engraving. (e) Surface microstructure of laser engraved hydroxyapatite surface using SEM, optical and 3D microscopes.

specimen (yellow dots) showed a statistically significant decrease compared with the cells attached to the HA region (gray dots), as shown in Fig. 3f and g.

A comparison of relative cell density mappings (Fig. 3h) of the laser-engraved area on Ti (inside of yellow dotted line) and the non-engraved area (outside of yellow dotted line) showed no significant difference, and no difference was found in the numerically measured cell density per distance in the laser-engraved area (red box) (Fig. 3i). On the other hand, a difference in density was clearly observed between the cells attached to the CMH area of the HA specimen (inside of yellow dotted line) and the cells on the surface without a CMH (outside of yellow dotted line) in the relative cell density maps (Fig. 3j). In addition, the cell density analysis showed a statistically significant decrease in the density of attached cells in the CMH region (Fig. 3k).

3.4. Acceleration of cell migration by CMH

The effect of the CMH on cell migration was determined by cell migration analysis with and without CMH implementation. When dispensing the cells, a masking film was used to prevent them from adhering to the patterned surface area so that only the effect on cell migration was observed, not the effect on cell adhesion (Fig. 4a). First, the migration characteristics of osteoblasts were confirmed on the laser-engraved Ti specimens with different widths. Fluorescence staining (cell nuclei, blue; cytoplasms, red) observation showed no difference in cell migration on the Ti surface with or without laser engraving (Fig. 4b). This is similar to the observed distributions of migrated cells in the laser-engraved area (yellow dots) and non-engraved area (gray dots) shown in Fig. 4d. The statistical significance test of the migration speed showed that there was no difference depending on the presence of laser engraving on the Ti surface, with cell migration rates of 286 ± 97 and 304 ± 99 μm/d, respectively (Fig. 4e). On the other hand, the CMH on the HA surface showed notably different characteristics. The cells in the CMH region migrated a far greater distance as observed by fluorescence microscopy (Fig. 4c). The cell migration rate in the CMH-free region was 203 ± 56 μm/d compared with 327 ± 91 μm/d in the CMH region, which is a 1.6-fold increase in average value and 3.2-fold increase in maximum value (Fig. 4g). In terms of relative cell density, there was no difference between the areas with and without laser engraving on the Ti surface (Fig. 4h). However, on the CMH surface, the cells were heavily concentrated in the CMH area (Fig. 4j). Interestingly, a closer look at the area where cells were concentrated on the CMH surface showed that they were mostly located in the boundary area between HA and the CMH, or the edge of the CMH (Fig. 4j). The dependence of the cell

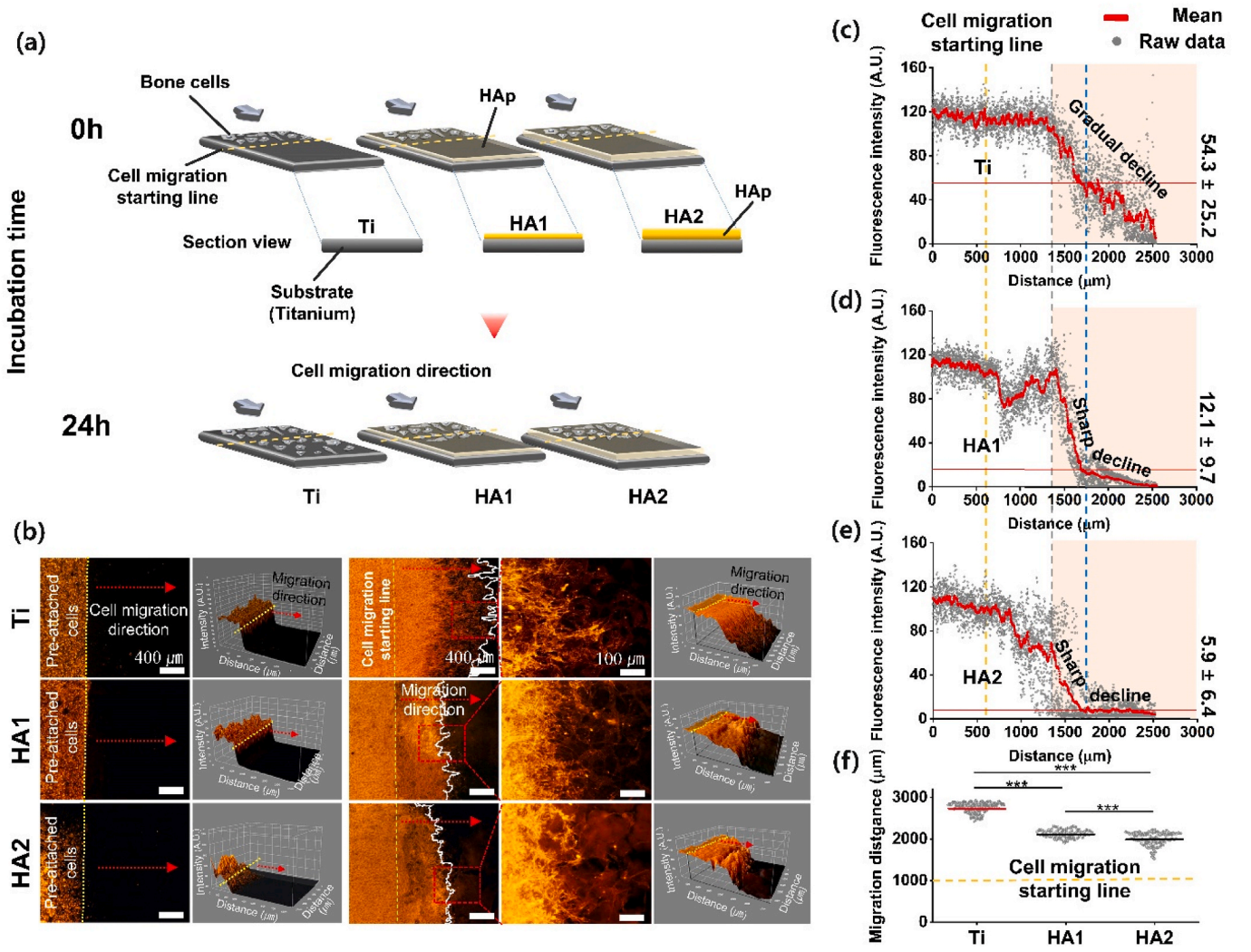

Fig. 2. Analysis of migration characteristics of bone cells depending on the thickness and presence of hydroxyapatite coating. (a) Schematic diagram of cell migration characteristics with (HA1, HA2) or without a hydroxyapatite coating (Ti) and depends on the hydroxyapatite coating's thickness (HA1, hydroxyapatite coating thickness; 16.8 ± 7.3μm), (HA2, hydroxyapatite coating thickness; 47.5 ± 12.7μm). (b) After migrating osteoblasts from each surface for 24 h, the cytoplasm was stained with fluorescence (Rodamine Phalloidin, Orange) and imaging with a microscope. The fluorescence intensity was compared by implementing three-dimensional fluorescence images. Numerical comparative analysis of fluorescence intensity according to the distance traveled when osteoblasts were cultured on each surface [(c) Ti (d), HA1 (e), HA2] for 24 h. (f) Analysis of statistical significance of cell migration distance (Data represent raw data and mean., *** indicate statistically significant difference when value compared to each comparison group with ***$P < 0.001$). (For interpretation of the references to color in this figure legend, the reader is referred to the Web version of this article.)

density characteristics on the presence of laser engraving or a CMH were also in good agreement with the findings discussed above in terms of statistical significance (Fig. 4i, k).

The laser engraving on the Ti surface and the CMH on the HA surface also showed different characteristics with changes in width. When the laser engraving width on the Ti surface was adjusted to 76 ± 4 (WD1), 144 ± 3 (WD2), and 248 ± 4 μm (WD3), the cell migration speeds were 277 ± 97, 304 ± 99, and 290 ± 105 μm/d, respectively. These are similar to that of the non-engraved area (282 ± 96 μm/d), indicating that there was no difference in cell migration speed upon adjusting the engraving width (Figs. S6b, f, j). On the other hand, in the CMH formed on HA, when the width was adjusted to 89 ± 6 (WD1), 175 ± 9 (WD2), and 241 ± 16 μm (WD3), the migration speeds were 256 ± 84, 323 ± 88, and 260 ± 85 μm/d, respectively. Compared with the speed of 202 ± 49 μm/d in the absence of a CMH, cell migration was faster in all CMHs, and adjusting the CMH width caused a significant difference in cell migration speed (Figs. S6d and h, l).

3.5. Analysis of cellular behavior in CMH through live cell observation

To understand the fundamentals of the CMH cell adhesion and migration speed characteristics, the cell behaviors were analyzed in the HA area (Fig. 5a), CMH area (Fig. 5h), and HA and CMH interfacial area (Fig. 5e) using a live cell microscope (Figs. S7 and S8). When the cell movements were tracked at 5 min intervals for 24 h, the cells in the HA region only moved within a relatively narrow region (Fig. 5b), whereas the cells in the CMH region moved around a wider region (Fig. 5i). The interfacial region between HA and the CMH showed intermediate characteristics of the HA and CMH regions (Fig. 5f). In terms of the cellular movement direction (Fig. S9), the cells in the HA and CMH regions did not tend toward a specific direction (Fig. 5c, j). Interestingly, however, the cells in the interfacial region tended to move toward the HA region (Fig. 5g). Comparison of the cell migration speeds showed that the HA region had the slowest movement while the CMH region had the fastest, and the interfacial region showed intermediate characteristics between the HA and CMH regions (Fig. 5d, k).

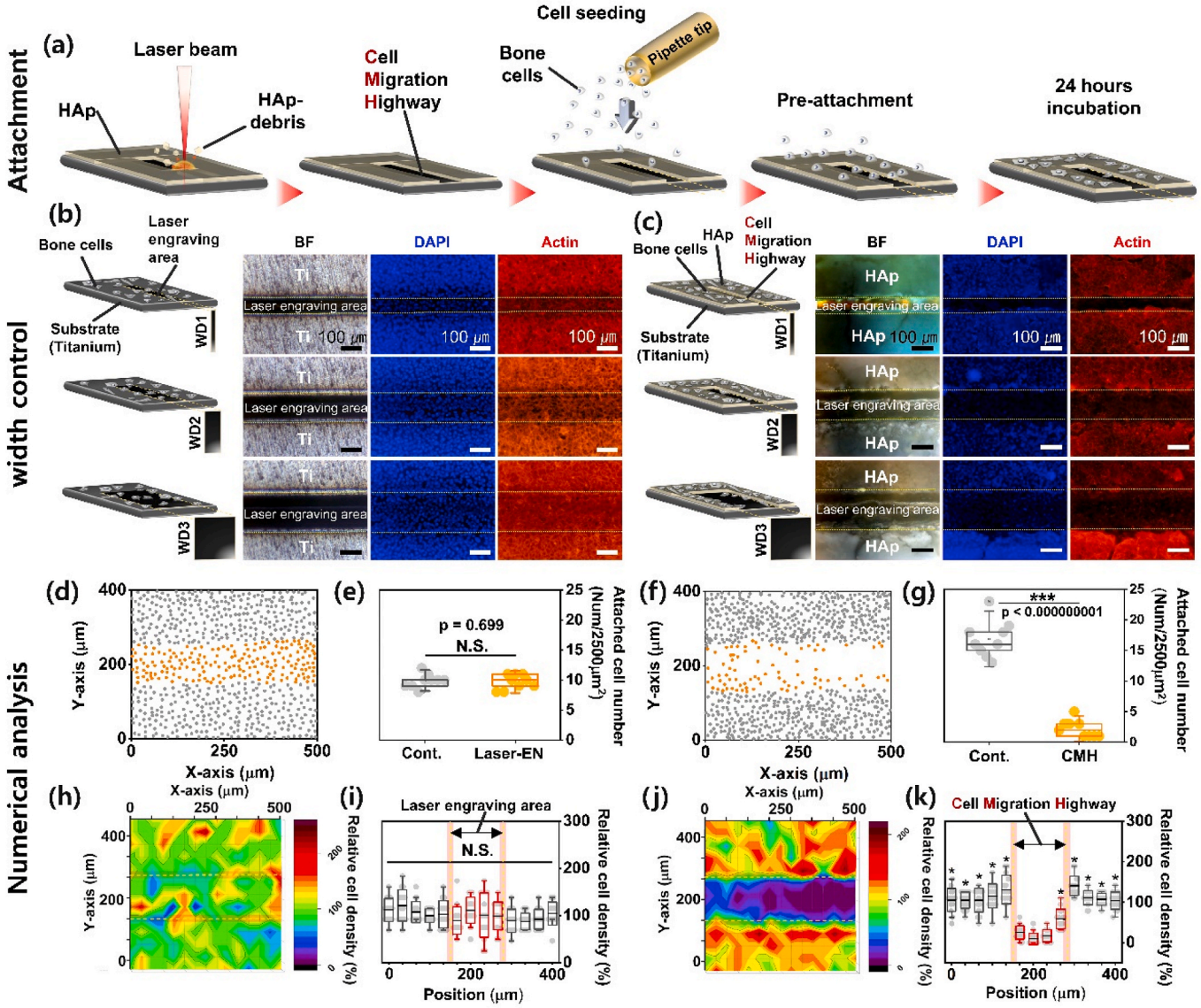

Fig. 3. Analysis of the adhesion characteristics of bone cells on the cell migration highway. (a) Schematic diagram to analyze osteoblasts adhesion characteristics on the surface of hydroxyapatite formed the cell migration highway pattern. (b) Different widths were formed by laser engraving on the titanium surface not coated with hydroxyapatite, and osteoblasts were cultured for 24 h to measure adhesion characteristics with a fluorescence microscope [BF; bright field image, DAPI; cell nucleus (blue), Actin; cytoplasm (red)]. (c) An image obtained by measuring osteoblasts adhesion under a fluorescence microscope after forming cell migration highways with different widths on the surface of hydroxyapatite. (d) Laser-engraved area and cell attachment location (yellow dot) in titanium without hydroxyapatite coating. Location and distribution of cells attached to the non-laser engraving area (gray dot). (e) Analysis of statistically significance of attachment number, (h) relative cell density map, and (i) numerical analysis graph of relative cell density. (f) Adhesion distribution of osteoblasts on the surface of the cell migration highway formed by laser engraving on the surface of hydroxyapatite. (g) Analysis of statistically significance of attachment number, (j) relative cell density map, and (k) numerical analysis graph of relative cell density. (Data represent raw data, mean and standard deviation., N.S. indicate not statistically significant., *, *** indicate statistically significant difference when value compared to each comparison group with * $P < 0.05$, ***$P < 0.0001$). (For interpretation of the references to color in this figure legend, the reader is referred to the Web version of this article.)

3.6. Cell migration characteristics of CMH through serum protein adhesion analysis

Serum protein adhesion was analyzed to understand the principle underlying the cell adhesion and migration characteristics of the CMH. When an implant material is placed in the body, the serum proteins first contact the material surface [39], and the amount and type of attached serum proteins are known to affect the adhesion and differentiation of bone-forming cells and bone formation [40,41]. In particular, fibronectin (FN) [42,43] and vitronectin (VN) [44,45] are known to promote the formation of focal adhesions of osteoblasts, resulting in favorable adhesion, proliferation, and differentiation of osteoblasts and ultimately bone formation [46–49].

FN and VN attached to the CMH and its surroundings were observed by immunostaining using a fluorescence microscope (Fig. 6a). The results confirmed that a significantly larger number of FN and VN attached to the HA region located around the CMH than to the CMH region itself (Fig. 6b, d, e). The amount of adhered serum proteins was also higher in the HA region than in the CMH region; this trend increased proportionally to the HA thickness (Fig. 6c).

The results indicate that the amount of adhered serum proteins, including FN and VN, is smaller in the CMH region than in the HA region, which might provide insights into the relatively low adhesion of osteoblasts and the accelerated cell migration. The amount of adhered

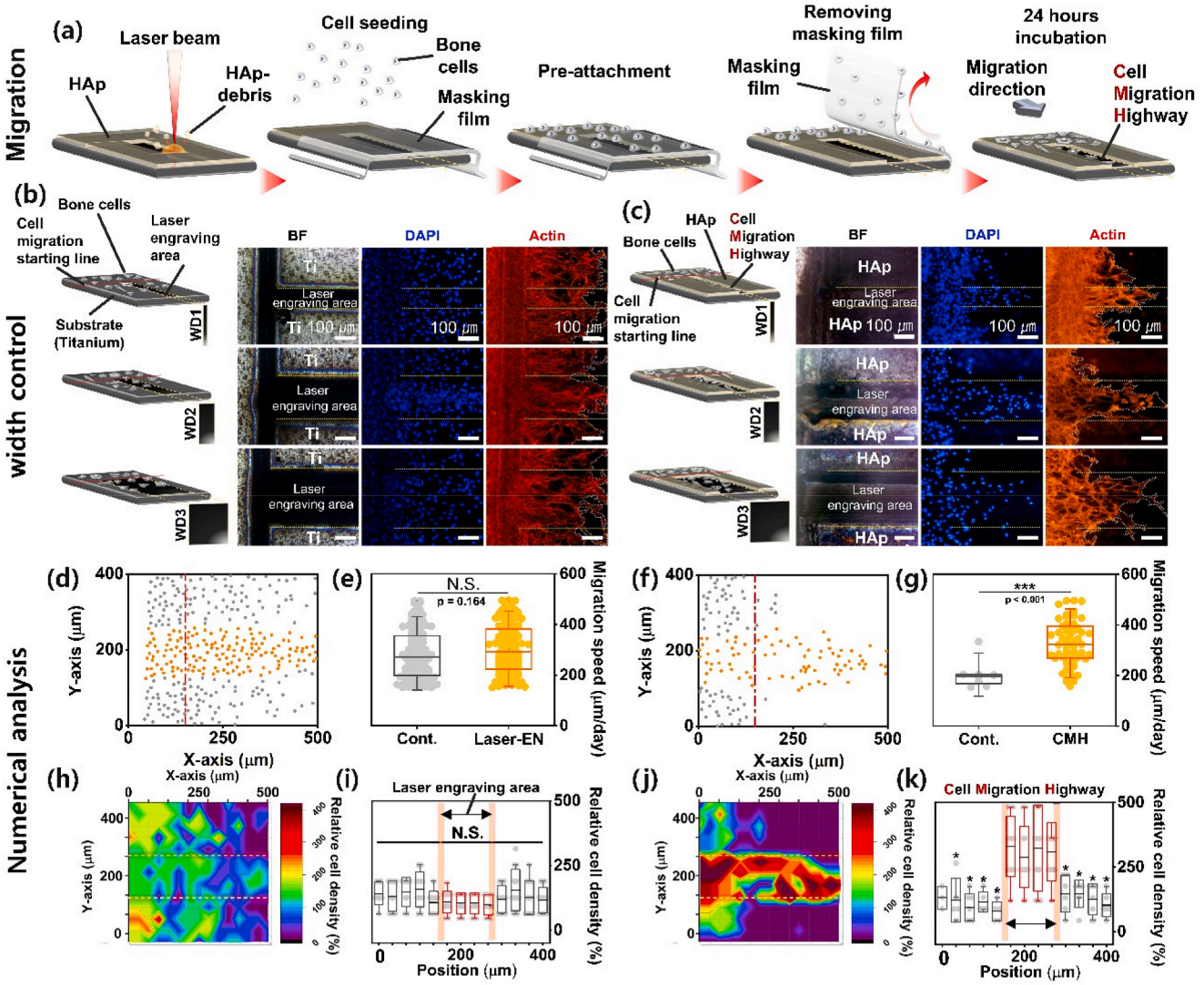

Fig. 4. Analysis of migration characteristics of bone cells on the cell migration highway. (a) A schematic diagram of analyzing the migration characteristics of osteoblasts on the hydroxyapatite surface formed the cell migration highway pattern. (b) Laser engraving on the titanium surface without hydroxyapatite coating to have a different width, and incubating osteoblasts for 24 h to determine migration characteristics by fluorescence microscopy [BF; bright field image, DAPI; cell nucleus (blue), Actin; cytoplasm (red)]. (c) A schematic diagram and images of observing migration by fluorescence microscopy by culturing osteoblasts 24 h after forming cell migration highways with different widths using laser engraving on the surface of hydroxyapatite. (d) Cell distribution on the surface of titanium without hydroxyapatite coating [Position of cells migrated to the laser-engraved area (yellow dot), cells migrated to the non-laser-engraved area (gray dot)]. Results of statistical significance analysis of migration speed (e), relative cell density map (h), and numerical analysis graph of relative cell density (i). Cell distribution on the cell migration highway of hydroxyapatite (f) [Position of cells migrated to the cell migration highway area (yellow dot), cells migrated to the non-cell migration highway area (gray dot)]. Results of statistical significance analysis of cell migration speed (g), mapping image of relative cell density (j), and statistical significance analysis of relative cell density (k). (Data represent raw data, mean and standard deviation., N.S. indicate not statistically significant., *, *** indicate statistically significant difference when value compared to each comparison group with * $P < 0.05$, ***$P < 0.0001$). (For interpretation of the references to color in this figure legend, the reader is referred to the Web version of this article.)

serum protein increased in proportion to the HA width, and observation of the cellular behavior around the CMH at different HA thicknesses confirmed that many cells gathered near the region where the amount of HA was relatively large (Fig. S10).

3.7. Analysis of the relationship between CMH width and cell attachment and migration

Analysis of the influence of cell adhesion and migration according to the width control of CMH was conducted. CMH with different widths was formed by laser engraving on the surface of the HA. The effect of laser surface treatment alone on cells was compared by engraving the titanium surface with the same laser conditions as CMH on HA (Fig. 7a). There was no difference in cell attachment between the non-lasered Ti surface and the laser engraved surface with adjusted width from WD1 to 3 (Fig. 7b). In contrast, CMH showed a decrease in cellular attachment for all of the width lengths from WD1∼3 compared to conventional HA. In particular, WD1 and WD2 showed a tendency to decrease cell attachment more than WD3 (Fig. 7c).

The effect of cell migration according to the adjustment of the laser engraving width was also analyzed. There was no statistically significant difference in cell migration for titanium surface with laser engraving width adjusted to WD1∼3 or non-lasered titanium (Fig. 7d). On the other hand, in CHM, all of WD1∼3 showed faster migration than HA, and in particular, WD2 showed the fastest migration speed.

Overall, the above results showed that the laser engraving on titanium does not change the adhesion and migration speed of cells. However, on the HA surface, cell adhesion and migration can be controlled

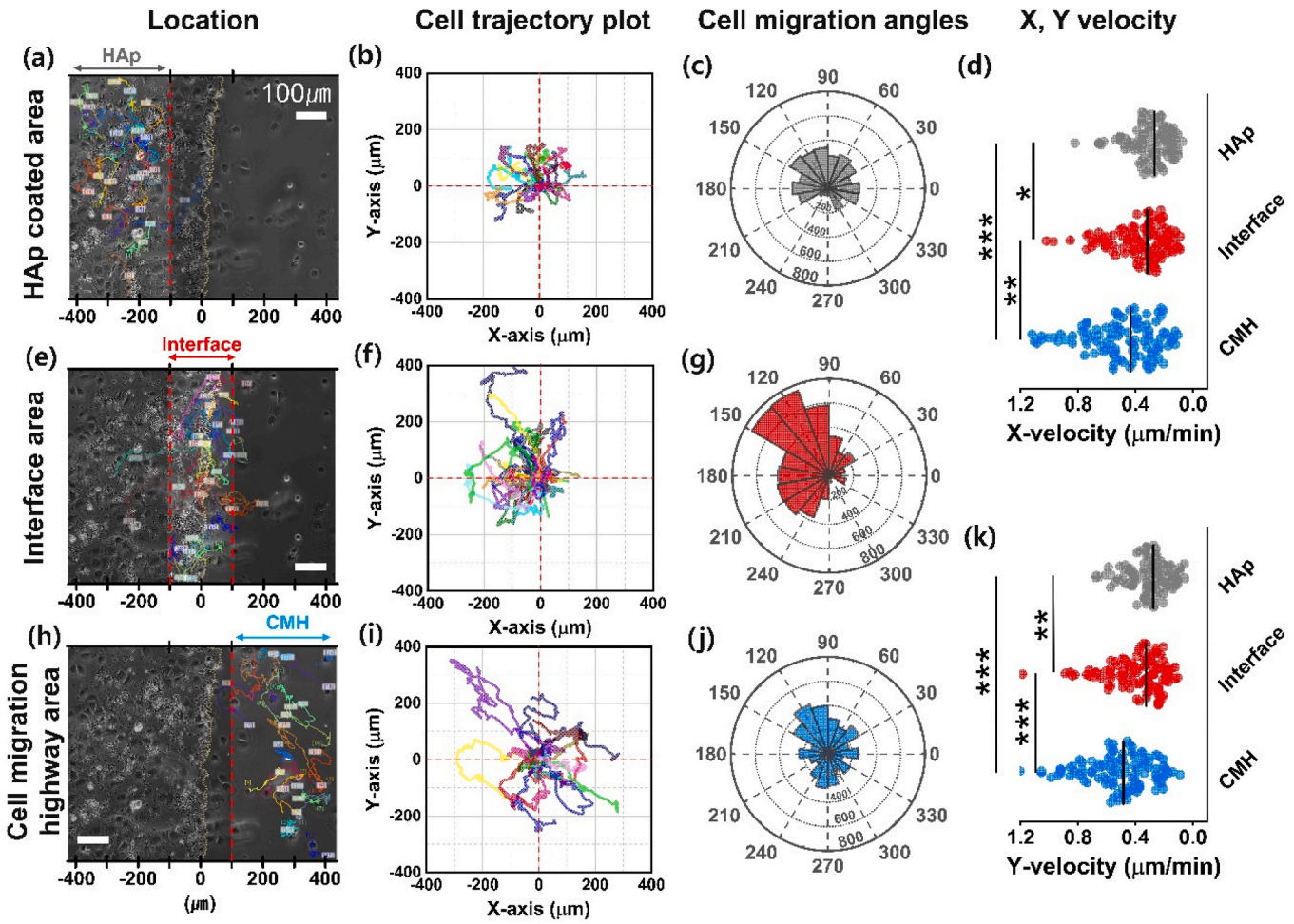

Fig. 5. Analysis of cell behavior in cell migration highway using live-cell observation and cell tracking. The behavior of osteoblasts in the hydroxyapatite coating area (a), the boundary area between the hydroxyapatite coating and the cell migration highway (e), and the cell migration highway area (h) for 24 h was observed through a live cell microscope, and the migration path was indicated. The result of tracking and analyzing the paths the cells traveled in the x- and y-axis in the hydroxyapatite coating area (b), the boundary area between the hydroxyapatite coating and the cell migration highway (f), and the cell migration highway area (i). The migration angle distribution of the cell migration direction characteristics on each surface [Hydroxyapatite coating area (c), boundary area between hydroxyapatite coating and cell migration highway (g), cell migration highway area (j)]. The velocity characteristics of the x-axis (d) and y-axis (k) of cell migration on each surface using a statistical significance method (Data represent raw data and mean., *, **, *** indicate statistically significant difference when value compared to each comparison group with * $P < 0.05$, **$P < 0.01$, ***$P < 0.0001$).

depending on the CMH width as well as the presence or absence of CMH.

4. Discussion

HA-coated on the titanium surface used in this study has a Ca/P ratio of 1.67 and has relatively low crystallinity [37]. Although it is known that the Ca/P ratio and crystallinity of HA affect the adhesion and growth of bone cells [58,59], this study studied the behavior of cells in the area where HA was removed through CMH. Therefore, it would be more appropriate to consider the effect of surface roughness, which is known to affect cell adhesion and migration, rather than the Ca/P ratio or crystallinity. The surface roughness of the HA-coated area was 7.66 ± 1.87 μm and 19.23 ± 6.38 μm in HA1 and HA2, respectively, and the titanium surface without HA coating was 0.15 ± 0.01 μm. Therefore, the HA surface showed a higher surface roughness value than the titanium surface (Fig. S1). However, there was no statistically significant difference in the surface roughness of the laser engraving area in which the cell response study was conducted, from 7.61 ± 0.49 μm to 7.50 ± 0.28 μm in titanium, and 7.94 ± 0.72 μm to 8.68 ± 1.33 μm in the CMH area implemented in HA (Fig. S1). Also, the effect of laser engraving on titanium and HA surfaces on cell adhesion and migration was compared. In titanium, the surface roughness of the non-laser engraving area increased to 0.15 ± 0.01 μm, and the treated area increased to 7.28 ± 0.31 μm. Still, there was no difference in cell adhesion and migration (Fig. 3 b,d,e,g,i and Fig. 4 b,d,e,h,i). Contrary to this, in the CMH region of HA, there was a difference in cell adhesion and migration in both the HA1 condition (7.66 ± 1.87μm) and HA2 (19.23 ± 6.38μm) (Fig. 3 c,f,g,j, k and Fig. 4 c,f,g,j,k). Therefore, it is presumed that the complex composition of HA and titanium is the main factor in controlling the adhesion and movement speed of cells by CMH, rather than surface roughness.

Chemotactic cell migration, in which cells try to move to locations with high concentrations of specific ions or proteins, has long been a well-known phenomenon [27,50–52]. Furthermore, osteoblasts have been reported to recognize chemical functional groups and serum proteins [53–55]. Osteoblasts have also been found to show reduced migration in areas with sufficient nutrients for growth [56], and when necessary components such as serum proteins are recognized, they tend to move toward them [57]. Taking these characteristics into consideration, the osteoblast cells located in the HA region are relatively rich in serum proteins (Fig. 6c–e), and thus they are reluctant to move to a different location (Fig. 7e and Figs. S6c and d). The CMH region is lacking in serum protein compared with the HA region (Fig. 6c–e), and thus the osteoblast cells seemed to move actively as a necessity to find a

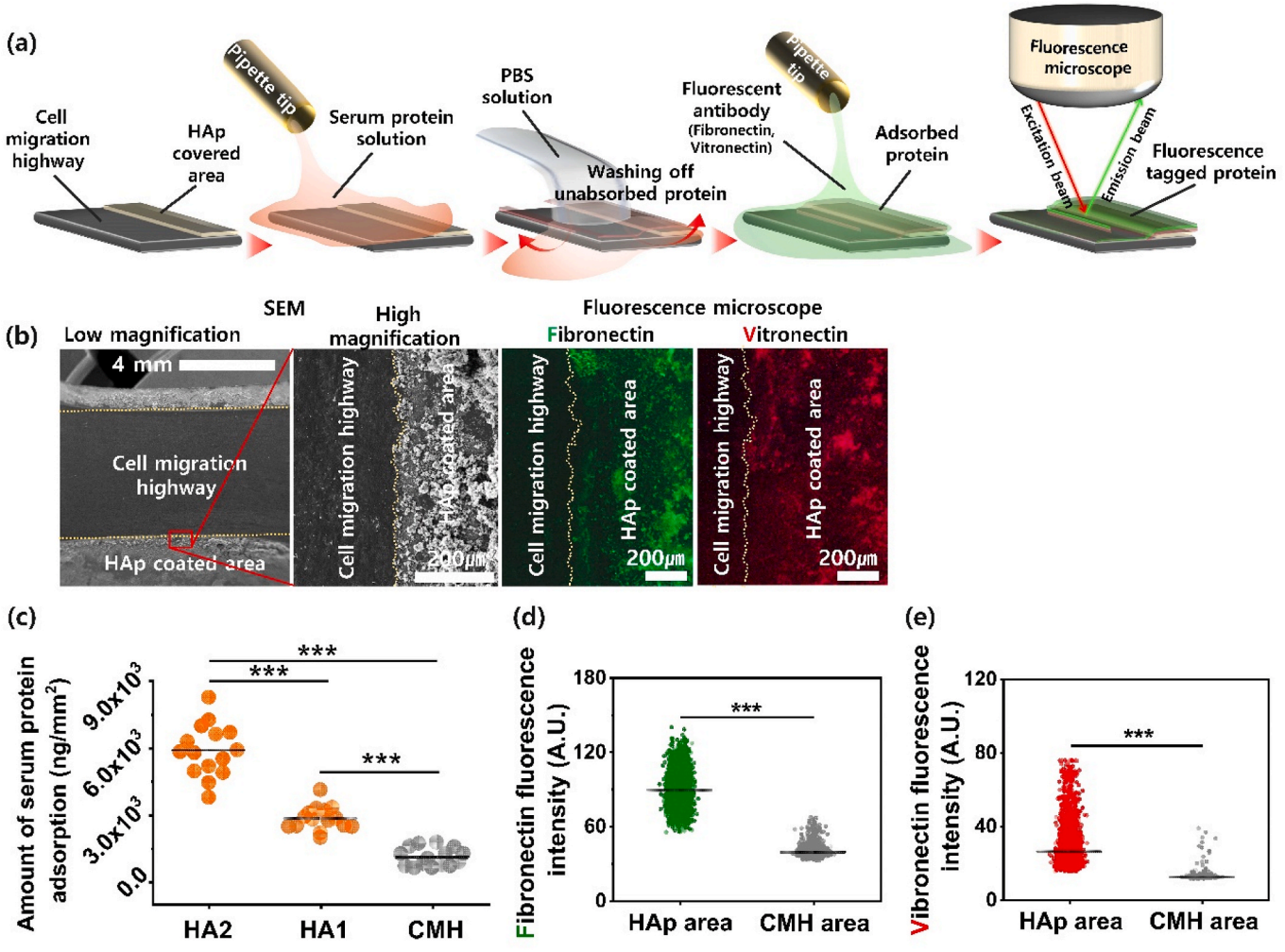

Fig. 6. Analysis of the causes of cell adhesion and migration characteristics on the cell migration highway. (a) Schematic diagram of the experimental procedure to analyze serum proteins adhesion properties on the cell migration highway. (b) The microstructure of the analysis site (cell migration highway region and hydroxyapatite region) to confirm the adhesion properties of serum proteins. Measurement image of the attached protein using a fluorescence microscope [fibronectin (green), vitronectin (red)]. (c) Comparing the total amount of serum proteins attached to the cell migration highway (CMH) region and the hydroxyapatite region (HA1, HA2). The statistical significance of the fluorescence intensities of fibronectin(d) and vitronectin(e) attached to the hydroxyapatite-coated area and the CMH area. (Data represent raw data and mean., *** indicate statistically significant difference when value compared to each comparison group with ***$P < 0.0001$). (For interpretation of the references to color in this figure legend, the reader is referred to the Web version of this article.)

better location (Fig. 7e and Figs. S6c and d).

Considering the cell behavior in the CMH region in more detail, the cells located at the interface adjacent to HA (within approximately 100 μm from the HA–CMH interface) tended to migrate to the HA region, which is relatively rich in serum proteins such as FN and VN (Fig. 5e–g). The cells located in the center of the CMH (approximately 100 μm apart from the HA–CMH interface) have access to a smaller amount of serum proteins attached to the surface, which makes them less likely to adhere, and they appear to move at relatively high speeds without a specific direction because they are far from the HA region (Fig. 5h–j, d, k).

As the cells use filopodia to recognize surrounding proteins and chemical components [60,61], and when spreading filopodia, the cell size is known to be 50–100 μm [62,63]. It is hypothesized that the distance at which the cells can recognize the high concentration of serum protein around them is within approximately 100 μm. Studies have shown that cells undergo directional migration when they detect concentration differences of surface ligand density [27]. When tracking the movement of cells in the HA-CMH region in real-time, most of the cells within 100 μm of the HA-CMH boundary region showed a tendency to migrate.

To verify this hypothesis, an evaluation of the cellular influence according to the CMH width was performed. The width of CMH was designed in three main ways: WD1 [100 or less, (89 ± 6 μm)], WD2 [100 to 200, (175 ± 9 μm)], and WD3 [200 or more, (241 ± 16 μm)]. We began pattern evaluation for 24 h with WD1, on which the cells were expected to have a high probability of meeting the HA surface after moving in a random direction. The width of the CMH was then increased for WD2 and WD3 for further investigation. The results indicate that the difference in the number of attached osteoblasts and their speed can be estimated according to the CMH width by the same hypothesis mentioned above. Comparing the number of adhered cells on the CMH depending on CMH width showed a statistically insignificant difference between WD1 and WD2, whereas the number of adhered cells increased on WD3 (Fig. 7c). On WD1 and WD2, the cells in the CMH region are relatively close to the HA region, which facilitates their migration to the latter. In contrast, on WD3, the cells are located far enough from the HA region to make it difficult for the cells to recognize it, causing many to remain in place. Analysis of the different numbers of cells attached to the surface showed an increase in cell density at the edge of the CMH (Fig. 3f, j, k and Figs. S11c, d, g, h, k, l), and live-cell microscopic observations and cell migration angle analysis also confirmed that cells located approximately 100 μm or less from the HA interface tended to

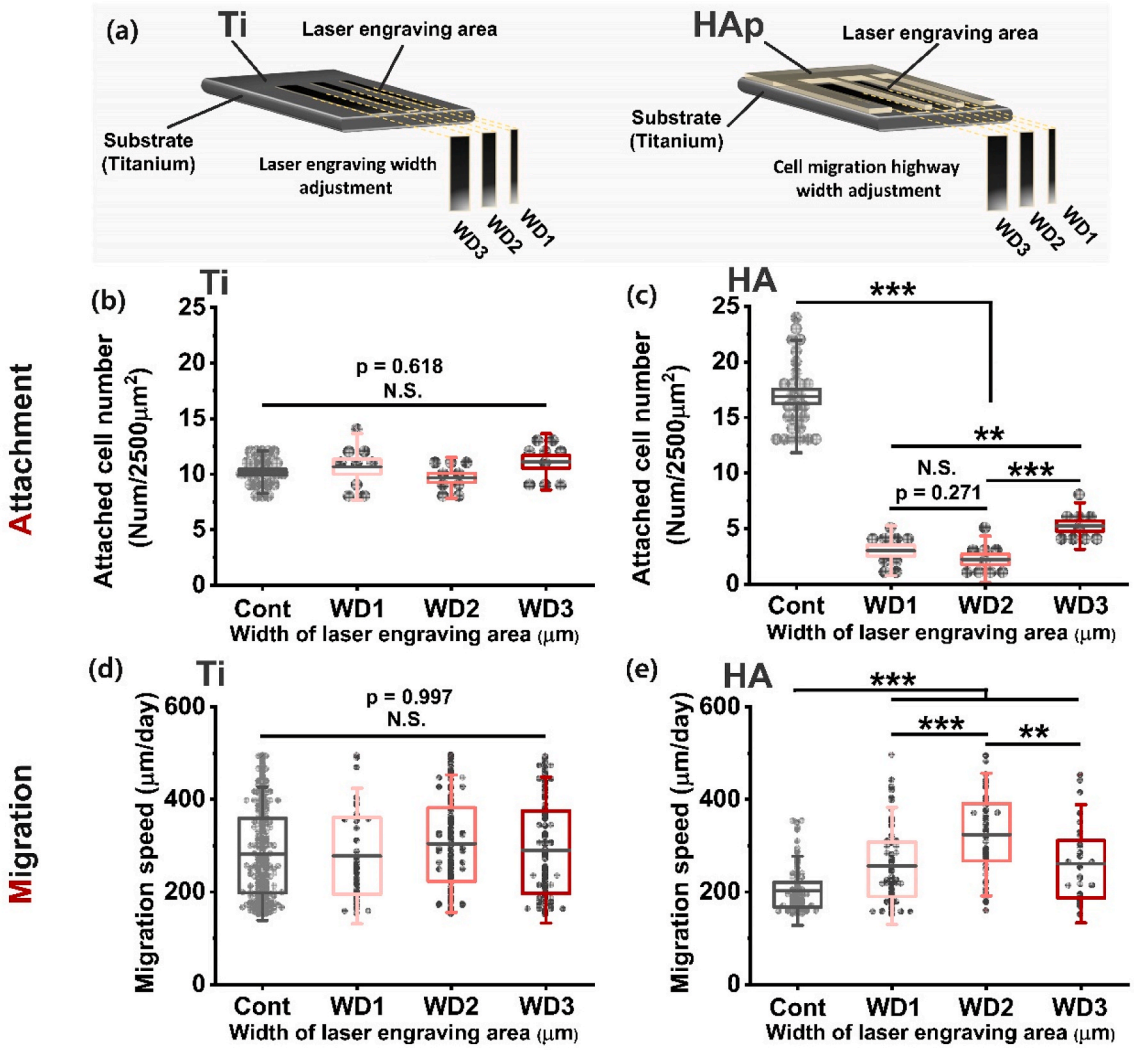

Fig. 7. Statistical significance analysis of the cell adhesion and migration effect according to laser engraving width. Numerical analysis of osteoblast adhesion properties (b), (c) and migration (d), (e) according to laser engraving width control on titanium specimens without a coating layer of hydroxyapatite (Ti) and specimens coated with hydroxyapatite (HA). (Ti: Cont; area without laser treatment, WD1; engraving width; 76±4 μm, WD2; engraving width; 144±3 μm, WD3; engraving width; 248±4 μm), (HA: Cont; area without laser treatment, WD1; engraving width; 89 ± 6μm, WD2; engraving width; 175 ± 9μm, WD3; engraving width; 241 ± 16μm). (Data represent raw data, mean and standard deviation., N.S. indicate not statistically significant., **, *** indicate statistically significant difference when value compared to each comparison group with **P < 0.01, ***P < 0.001).

migrate toward the HA region (Mov. S2 and Fig. 5g). In contrast, cells 100 μm or farther moved randomly rather than toward the HA region (Mov. S3 and Fig. 5j).

Supplementary video related to this article can be found at https://doi.org/10.1016/j.bioactmat.2021.03.025

Based on the above results, the mechanism underlying the difference in cell migration speeds according to CMH width could also be estimated. The cells on WD1 tended to migrate toward the HA area rather than remain in the CMH area, and thus the number of cells attached to the CMH area was relatively small and the migration speed was relatively low (Figs. S4c and d and Figs. S6c and d). The cells on WD3 were farther from HA, enabling them to move freely, but they appeared to be too far from a location with sufficient attached serum proteins, which in turn discouraged continuous migration (Fig. S4k, l and Figs. S6k and l). On the contrary, the cells on WD2 could recognize the HA region where abundant serum proteins, including FN and VN, were attached. When the cells are not too far from the HA region, it is presumed that the chemotaxis of attempting to find locations with high serum protein contents at detectable distances serves as potential for continuous migration, enabling the cells to move toward the nearby HA region.

The CMH was able to control cell adhesion and migration speed according to its width (Figs. 3, 4, 7 and S4, S5, S6). Specifically, cell adhesion was promoted on the surface of the narrow width CMH or the HA (Fig. 7b, c and Figs. S4d, h, i). The cell migration rate was not proportional to the CMH width but was maximized at a specific width (Fig. 7d, e and Figs. S6d, h, i). From these results, it is expected that the adhesion and migration of cells on the implant surface can be controlled by adjusting the width and spacing of CMH on the HA-coated surface.

5. Conclusion

The surfaces of various implants that require direct bonding with bone are often coated with HA, which contains calcium and phosphorus, to increase the bonding strength. However, while cell adhesion is promoted on the HA surface, cell movement is inhibited due to strong adhesion, which inhibits the even spread of osteogenic cells on the surface of the implant material. The implementation of a CMH pattern promotes cell migration using only laser processing on the surface of existing HA without any complicated additional processes. The CMH implementation technique allows for a road-type topography and the

simultaneous exposure of two different implant materials with different surface properties. Compared with the conventional HA surface without a pattern, the CMH could promote the movement of bone-forming cells and control the adhesion and speed of the cells according to the CMH width. Based on the results, designing a patterned surface that can appropriately control bone adhesion or bone cell movement is possible by adjusting the ratio or pattern shape of the interfacial surface area where HA and the exposed parent material coexist through laser engraving. In this study, we developed a technique for implementing patterning on the HA surface and confirmed that such pattern could regulate cell adhesion and migration at the cellular level. The cause of this phenomenon was explained through the analysis of proteins related to bone formation. Based on the findings presented in this study, a follow-up study is needed to implement developed patterns in various materials and confirm the in vivo effect through animal experiments. However, since this technique can be applied to all apatite materials and materials with apatite coatings through a simple laser process, it could soon act as a gateway to expanding the field of material implantations.

Declaration of competing InterestCOI

The authors declare no competing financial interests or personal relationships.

CRediT authorship contribution statement

Seung-Hoon Um: Experiment design, Data acquisition & analysis, Writing. **Jaehong Lee:** Data acquisition, Data analysis, Conceptualization. **In-Seok Song:** Supervision, Conceptualization, Funding acquisition. **Myoung-Ryul Ok:** Supervision, Conceptualization, Funding acquisition. **Yu-Chan Kim:** Supervision, Conceptualization, Funding acquisition. **Hyung-Seop Han:** Supervision, Conceptualization, Methodology, Writing – review & editing. **Sang-Hoon Rhee:** Supervision, Conceptualization, Methodology. **Hojeong Jeon:** Supervision, Writing – review & editing, Funding acquisition.

Acknowledgments

This work was supported by a National Research Foundation of Korea (NRF) grant funded by the Korean government (MSIT) [grant number 2020R1A2C2010413], the Korea Medical Device Development Fund grant funded by the Korea government (the Ministry of Science and ICT, the Ministry of Trade, Industry and Energy, the Ministry of Health & Welfare, the Ministry of Food and Drug Safety) (NTIS Number:9991007189), the KIST project (grant number 2E31121), and the KU-KIST Graduate School of Converging Science and Technology Program.

Appendix A. Supplementary data

Supplementary data to this article can be found online at https://doi.org/10.1016/j.bioactmat.2021.03.025.

References

[1] O.A. Tertuliano, J.R. Greer, The nanocomposite nature of bone drives its strength and damage resistance, Nat. Mater. 15 (2016) 1195–1202.
[2] S. Von Euw, Y. Wang, G. Laurent, C. Drouet, F. Babonneau, N. Nassif, T. Azaïs, Bone mineral: new insights into its chemical composition, Sci. Rep. 9 (2019) 8456.
[3] W.S.W. Harun, R.I.M. Asri, J. Alias, F.H. Zulkifli, K. Kadirgama, S.A.C. Ghani, J.H. M. Shariffuddin, A comprehensive review of hydroxyapatite-based coatings adhesion on metallic biomaterials, Ceram. Int. 44 (2018) 1250–1268.
[4] H. Samadian, H. Mobasheri, M. Azami, R. Faridi-Majidi, Osteoconductive and electroactive carbon nanofibers/hydroxyapatite nanocomposite tailored for bone tissue engineering: in vitro and in vivo studies, Sci. Rep. 10 (2020) 14853.
[5] D. Ke, A.A. Vu, A. Bandyopadhyay, S. Bose, Compositionally graded doped hydroxyapatite coating on titanium using laser and plasma spray deposition for bone implants, Acta Biomater. 84 (2019) 414–423.
[6] P. Habibovic, F. Barrère, C.A. Van Blitterswijk, K. de Groot, P. Layrolle, Biomimetic hydroxyapatite coating on metal implants, J. Am. Ceram. Soc. 85 (2002) 517–522.
[7] J.R. Alhamdi, T. Peng, I.M. Al-Naggar, K.L. Hawley, K.L. Spiller, L.T. Kuhn, Controlled M1-to-M2 transition of aged macrophages by calcium phosphate coatings, Biomaterials 196 (2019) 90–99.
[8] B.-D. Sui, C.-H. Hu, A.-Q. Liu, C.-X. Zheng, K. Xuan, Y. Jin, Stem cell-based bone regeneration in diseased microenvironments: challenges and solutions, Biomaterials 196 (2019) 18–30.
[9] K. Anselme, Osteoblast adhesion on biomaterials, Biomaterials 21 (2000) 667–681.
[10] S. Chen, Y. Guo, R. Liu, S. Wu, J. Fang, B. Huang, Z. Li, Z. Chen, Z. Chen, Tuning surface properties of bone biomaterials to manipulate osteoblastic cell adhesion and the signaling pathways for the enhancement of early osseointegration, Colloids Surf., B 164 (2018) 58–69.
[11] X. Cui, T. Murakami, Y. Tamura, K. Aoki, Y. Hoshino, Y. Miura, Bacterial inhibition and osteoblast adhesion on Ti alloy surfaces modified by poly(PEGMA-r-phosmer) coating, ACS Appl. Mater. Interfaces 10 (2018) 23674–23681.
[12] Y. Su, I. Cockerill, Y. Zheng, L. Tang, Y.-X. Qin, D. Zhu, Biofunctionalization of metallic implants by calcium phosphate coatings, Bioact. Mater. 4 (2019) 196–206.
[13] R.A. Surmenev, M.A. Surmeneva, A critical review of decades of research on calcium phosphate–based coatings: how far are we from their widespread clinical application? Curr. Opin. Biomed. Eng. 10 (2019) 35–44.
[14] G. Choi, A.H. Choi, L.A. Evans, S. Akyol, B. Ben-Nissan, A review: recent advances in sol-gel-derived hydroxyapatite nanocoatings for clinical applications, J. Am. Ceram. Soc. 103 (2020) 5442–5453.
[15] L.-C. Zhang, L.-Y. Chen, A review on biomedical titanium alloys: recent progress and prospect, Adv. Eng. Mater. 21 (2019) 1801215.
[16] K.F. Eichholz, S. Von Euw, R. Burdis, D.J. Kelly, D.A. Hoey, Development of a new bone-mimetic surface treatment platform: nanoneedle hydroxyapatite (nnHA) coating, Adv. Healthc. Mater. 9 (2020) 2001102.
[17] G. Wei, C. Gong, K. Hu, Y. Wang, Y. Zhang, Biomimetic hydroxyapatite on graphene supports for biomedical applications: a review, Nanomaterials 9 (2019) 1435.
[18] M.S. Lee, D.H. Lee, J. Jeon, S.H. Oh, H.S. Yang, Topographically defined, biodegradable nanopatterned patches to regulate cell fate and acceleration of bone regeneration, ACS Appl. Mater. Interfaces 10 (2018) 38780–38790.
[19] G. Yang, H. Liu, Y. Cui, J. Li, X. Zhou, N. Wang, F. Wu, Y. Li, Y. Liu, X. Jiang, S. Zhang, Bioinspired membrane provides periosteum-mimetic microenvironment for accelerating vascularized bone regeneration, Biomaterials 268 (2021) 120561.
[20] M. Mebarki, L. Coquelin, P. Layrolle, S. Battaglia, M. Tossou, P. Hernigou, H. Rouard, N. Chevallier, Enhanced human bone marrow mesenchymal stromal cell adhesion on scaffolds promotes cell survival and bone formation, Acta Biomater. 59 (2017) 94–107.
[21] R. Setiawati, P. Rahardjo, Bone development and growth, in: BoD–Books on Demand, 2019.
[22] C.W. Peak, K.A. Singh, M.a. Adlouni, J. Chen, A.K. Gaharwar, Printing therapeutic proteins in 3D using nanoengineered bioink to control and direct cell migration, Adv. Healthc. Mater. 8 (2019) 1801553.
[23] E.H. Barriga, K. Franze, G. Charras, R. Mayor, Tissue stiffening coordinates morphogenesis by triggering collective cell migration in vivo, Nature 554 (2018) 523–527.
[24] S. Van Helvert, C. Storm, P. Friedl, Mechanoreciprocity in cell migration, Nat. Cell Biol. 20 (2018) 8.
[25] M.S. Carvalho, J.M. Cabral, C.L. da Silva, D. Vashishth, Synergistic effect of extracellularly supplemented osteopontin and osteocalcin on stem cell proliferation, osteogenic differentiation, and angiogenic properties, J. Cell. Biochem. 120 (2019) 6555–6569.
[26] J. Wei, J. Shimazu, Munevver P. Makinistoglu, A. Maurizi, D. Kajimura, H. Zong, T. Takarada, T. Iezaki, Jeffrey E. Pessin, E. Hinoi, G. Karsenty, Glucose uptake and Runx2 synergize to orchestrate osteoblast differentiation and bone formation, Cell 161 (2015) 1576–1591.
[27] H. Jeon, S. Koo, W.M. Reese, P. Loskill, C.P. Grigoropoulos, K.E. Healy, Directing cell migration and organization via nanocrater-patterned cell-repellent interfaces, Nat. Mater. 14 (2015) 918–923.
[28] B. Hu, W.R. Leow, S. Amini, B. Nai, X. Zhang, Z. Liu, P. Cai, Z. Li, Y.-L. Wu, A. Miserez, C.T. Lim, X. Chen, Orientational coupling locally orchestrates a cell migration pattern for Re-epithelialization, Adv. Mater. 29 (2017) 1700145.
[29] F.M. Refaaq, X. Chen, S.W. Pang, Effects of topographical guidance cues on osteoblast cell migration, Sci. Rep. 10 (2020) 20003.
[30] M. Ermis, E. Antmen, V. Hasirci, Micro and Nanofabrication methods to control cell-substrate interactions and cell behavior: a review from the tissue engineering perspective, Bioact. Mater. 3 (2018) 355–369.
[31] L. Ge, L. Yang, R. Bron, J.K. Burgess, P. van Rijn, Topography-mediated fibroblast cell migration is influenced by direction, wavelength, and amplitude, ACS Appl. Bio Mater. 3 (2020) 2104–2116.
[32] C. Zhao, X. Wang, L. Gao, L. Jing, Q. Zhou, J. Chang, The role of the micro-pattern and nano-topography of hydroxyapatite bioceramics on stimulating osteogenic differentiation of mesenchymal stem cells, Acta Biomater. 73 (2018) 509–521.
[33] I.-G. Kang, C.-I. Park, Y.-J. Seong, H. Lee, H.-E. Kim, C.-M. Han, Bioactive and mechanically stable hydroxyapatite patterning for rapid endothelialization of artificial vascular graft, Mater. Sci. Eng. C 106 (2020) 110287.
[34] K. Rabel, R.-J. Kohal, T. Steinberg, P. Tomakidi, B. Rolauffs, E. Adolfsson, P. Palmero, T. Fürderer, B. Altmann, Controlling osteoblast morphology and proliferation via surface micro-topographies of implant biomaterials, Sci. Rep. 10 (2020) 12810.
[35] T. Akasaka, H. Miyaji, N. Kaga, A. Yokoyama, S. Abe, Y. Yoshida, Adhesion of osteoblast-like cells (Saos-2) on micro-/submicro-patterned apatite scaffolds

fabricated with apatite cement paste by micro-molding, Nano Biomed 8 (2016) 112–122.
[36] A. Sikora, G. Coustillier, T. Sarnet, M. Sentis, Laser engraving optimization for achieving smooth sidewalls, Appl. Surf. Sci. 492 (2019) 382–391.
[37] S.-H. Um, Y.-W. Chung, Y. Seo, H. Seo, M.-R. Ok, Y.-C. Kim, H.-S. Han, J.J. Chung, J.R. Edwards, H. Jeon, Robust hydroxyapatite coating by laser-induced hydrothermal synthesis, Adv. Funct. Mater. 30 (2020) 2005233.
[38] F. Piccinini, A. Kiss, P. Horvath, CellTracker (not only) for dummies, Bioinformatics 32 (2015) 955–957.
[39] M. Talha, Y. Ma, P. Kumar, Y. Lin, A. Singh, Role of protein adsorption in the bio corrosion of metallic implants–A review, Colloids Surf., B 176 (2019) 494–506.
[40] J. Wang, X. Chen, B. Guo, X. Yang, Y. Zhou, X. Zhu, K. Zhang, Y. Fan, C. Tu, X. Zhang, A serum protein adsorption profile on BCP ceramics and influence of the elevated adsorption of adhesive proteins on the behaviour of MSCs, J. Mater. Chem. B 6 (2018) 7383–7395.
[41] A. Toffoli, L. Parisi, M.G. Bianchi, S. Lumetti, O. Bussolati, G.M. Macaluso, Thermal treatment to increase titanium wettability induces selective proteins adsorption from blood serum thus affecting osteoblasts adhesion, Mater. Sci. Eng. C 107 (2020) 110250.
[42] K.M. Yamada, K. Olden, Fibronectins—adhesive glycoproteins of cell surface and blood, Nature 275 (1978) 179–184.
[43] J. Patten, K. Wang, Fibronectin in development and wound healing, Adv. Drug Deliv. Rev. 170 (2021) 353–368.
[44] T. Li, L. Hao, J. Li, C. Du, Y. Wang, Insight into vitronectin structural evolution on material surface chemistries: the mediation for cell adhesion, Bioact. Mater. 5 (2020) 1044–1052.
[45] S.-K. Min, H.K. Kang, S.Y. Jung, B.-M. Min, A vitronectin-derived peptide reverses ovariectomy-induced bone loss via regulation of osteoblast and osteoclast differentiation, Cell Death Differ. 25 (2018) 268–281.
[46] H.P. Felgueiras, M.D. Evans, V. Migonney, Contribution of fibronectin and vitronectin to the adhesion and morphology of MC3T3-E1 osteoblastic cells to poly (NaSS) grafted Ti6Al4V, Acta Biomater. 28 (2015) 225–233.
[47] L. Parisi, A. Toffoli, B. Ghezzi, B. Mozzoni, S. Lumetti, G.M. Macaluso, A glance on the role of fibronectin in controlling cell response at biomaterial interface, Jpn Dent Sci Rev 56 (2020) 50–55.
[48] M. Griffin, A. Ibrahim, A. Seifalian, P. Butler, D. Kalaskar, P. Ferretti, Chemical group-dependent plasma polymerisation preferentially directs adipose stem cell differentiation towards osteogenic or chondrogenic lineages, Acta Biomater. 50 (2017) 450–461.
[49] S. Trujillo, C. Gonzalez-Garcia, P. Rico, A. Reid, J. Windmill, M.J. Dalby, M. Salmeron-Sanchez, Engineered 3D hydrogels with full-length fibronectin that sequester and present growth factors, Biomaterials 252 (2020) 120104.
[50] D.A. Lauffenburger, A.F. Horwitz, Cell migration: a physically integrated molecular process, Cell 84 (1996) 359–369.
[51] B. Lin, T. Yin, Y.I. Wu, T. Inoue, A. Levchenko, Interplay between chemotaxis and contact inhibition of locomotion determines exploratory cell migration, Nat. Commun. 6 (2015) 1–14.
[52] H. Jeon, R. Schmidt, J.E. Barton, D.J. Hwang, L.J. Gamble, D.G. Castner, C. P. Grigoropoulos, K.E. Healy, Chemical patterning of ultrathin polymer films by direct-write multiphoton lithography, J. Am. Chem. Soc. 133 (2011) 6138–6141.
[53] A. El-Ghannam, P. Ducheyne, I. Shapiro, Effect of serum proteins on osteoblast adhesion to surface-modified bioactive glass and hydroxyapatite, J. Orthop. Res. 17 (1999) 340–345.
[54] B.D. Riehl, J.S. Lee, L. Ha, I.K. Kwon, J.Y. Lim, Flowtaxis of osteoblast migration under fluid shear and the effect of RhoA kinase silencing, PloS One 12 (2017), e0171857.
[55] A. Broz, E. Ukraintsev, A. Kromka, B. Rezek, M. Hubalek Kalbacova, Osteoblast adhesion, migration, and proliferation variations on chemically patterned nanocrystalline diamond films evaluated by live-cell imaging, J. Biomed. Mater. Res. 105 (2017) 1469–1478.
[56] H. Pahwa, M.T. Khan, K. Sharan, Hyperglycemia impairs osteoblast cell migration and chemotaxis due to a decrease in mitochondrial biogenesis, Mol. Cell. Biochem. 469 (2020) 109–118.
[57] A. Thiel, M.K. Reumann, A. Boskey, J. Wischmann, R. von Eisenhart-Rothe, P. Mayer-Kuckuk, Osteoblast migration in vertebrate bone, Biol. Rev. 93 (2018) 350–363.
[58] H. Liu, H. Yazici, C. Ergun, T.J. Webster, H. Bermek, An in vitro evaluation of the Ca/P ratio for the cytocompatibility of nano-to-micron particulate calcium phosphates for bone regeneration, Acta Biomater. 4 (2008) 1472–1479.
[59] H. Nagai, M. Kobayashi-Fujioka, K. Fujisawa, G. Ohe, N. Takamaru, K. Hara, D. Uchida, T. Tamatani, K. Ishikawa, Y. Miyamoto, Effects of low crystalline carbonate apatite on proliferation and osteoblastic differentiation of human bone marrow cells, J. Mater. Sci.: Mater. 26 (2015) 99.
[60] LIM, Yul Jung, Henry J. Donahue, Cell sensing and response to micro-and nanostructured surfaces produced by chemical and topographic patterning, Tissue Eng. 13 (2007) 1879–1891.
[61] M.J. Dalby, L. Di Silvio, N. Gurav, B. Annaz, M.V. Kayser, W. Bonfield, Optimizing HAPEX™ topography influences osteoblast response, Tissue Eng. 8 (2002) 453–467.
[62] D.C. Pirapaharan, J.B. Olesen, T.L. Andersen, S.B. Christensen, P. Kjærsgaard-Andersen, J.-M. Delaisse, K. Søe, Catabolic activity of osteoblast lineage cells contributes to osteoclastic bone resorption in vitro, J. Cell Sci. 132 (2019) 10.
[63] I. Izquierdo-Barba, J.M. García-Martín, R. Álvarez, A. Palmero, J. Esteban, C. Pérez-Jorge, D. Arcos, M. Vallet-Regí, Nanocolumnar coatings with selective behavior towards osteoblast and Staphylococcus aureus proliferation, Acta Biomater. 15 (2015) 20–28.